Novel Parameter Identification Method for Basis Weight Control Loop of Papermaking Process

Yunzhu Shen[1], Wei Tang[1,*], Yungang Liu[2]

1. *School of Electrical and Control Engineering, Shaanxi University of Science and Technology, Xi'an, Shaanxi Province,* 710021*, China*

2. *School of Control Science and Engineering, Shandong University, Ji'nan, Shandong Province,* 250061*, China*

Abstract: The basis weight control loop of the papermaking process is a non-linear system with time-delay and time-varying. It is impractical to identify a model that can restore the model of real papermaking process. Determining a more accurate identification model is very important for designing the controller of the control system and maintaining the stable operation of the papermaking process. In this study, a strange nonchaotic particle swarm optimization (SNPSO) algorithm is proposed to identify the models of real papermaking processes, and this identification ability is significantly enhanced compared with particle swarm optimization (PSO). First, random particles are initialized by strange nonchaotic sequences to obtain high-quality solutions. Furthermore, the weight of linear attenuation is replaced by strange nonchaotic sequence and the time-varying acceleration coefficients and a mutation rule with strange nonchaotic characteristics are utilized in SNPSO. The above strategies effectively improve the global and local search ability of particles and the ability to escape from local optimization. To illustrate the effectiveness of SNPSO, step response data are used to identify the models of real industrial processes. Compared with classical PSO, PSO with time-varying acceleration coefficients (PSO-TVAC) and modified particle swarm optimization (MPSO), the simulation results demonstrate that SNPSO has stronger identification ability, faster convergence speed, and better robustness.

Keywords: basis weight control system; papermaking; system identification; particle swarm optimization; strange nonchaotic sequence

DOI: 10.26599/PBM.2023.9260004

Yunzhu Shen, PhD candidate;
E-mail: jdshenyunzhu@163.com

*Corresponding author:
Wei Tang, professor, PhD tutor;
research interest: papermaking automation;
E-mail: wtang906@163.com

Received: 14 November 2022; accepted: 24 December 2022.

1 Introduction

The basis weight control loop of the papermaking process has the characteristics of large time-delay and external interference; hence, it is difficult to establish an accurate mathematical model [1]. Previous studies [2–3] have demonstrated that its model is usually approximated to a low-order transfer function with time-delay, including first-order-plus-dead-time (FOPDT) or second-order-plus-dead-time (SOPDT) structures. Because these models not only effectively reflect the basic dynamics of the paper industry process, they can also contribute to the design of the controller. With the extensive use of model-based advanced control methods in the papermaking process, the high-precision identification of models is one of the challenges that urgently needs to be solved in the control field. Therefore, it is very important to identify the FOPDT or SOPDT models for designing the controller and maintaining stable operation of the papermaking process.

Several effective system identification techniques [4–9] have been proposed. The least square method (LSM) [10] is an effective method to identify models of time-delay. This method is an identification algorithm based on discrete systems; therefore, the continuous transfer function needs to be discretized. The improper selection of sampling intervals and non-integer optimization problem of systems with time-delay can increase the difficulty of identification. A frequency domain identification method [11] is proposed to identify the parameters of a system with time-delay. It requires a small amount of calculation and strong robustness, but ignores the high-frequency dynamics of the system, and is easy to converge locally. Filter-based adaptive identification algorithm [12] is the most commonly employed method to identify time-delay systems and avoid local minima under full excitation; however, full excitation is not suitable for practical industrial processes. Therefore, it is meaningful to determine a system identification method with strong identification ability, good robustness, and suitable for engineering practice.

Recently, intelligent optimization technologies have garnered significant attention in system identification [13–17]. One of the most popular optimization algorithms for system identification is particle swarm optimization (PSO)-based algorithm [18]. PSO algorithm is a population-based optimization algorithm introduced by Kennedy and Eberhart in 1995 [19]. It is used to identify time-delay model parameters and achieved good results [20]. However, classical PSO is easily classified as local optimal value and its local search ability is relatively poor. To improve the performance of PSO algorithm, various versions of the improved PSO algorithm have been proposed. Zou et al [21] proposed an improved PSO algorithm to identify the infinitive impulse response (IIR) system. Using the golden section rate to divide the solution space, different inertia weights and normal distribution improve the global search ability and convergence speed of the algorithm to obtain high-quality solutions. Feng et al [22] proposed a modified PSO algorithm to identify micro piezoelectric actuators. This method improves the ability of global optimization and ensures the accuracy of parameter identification.

Strange nonchaos [23–28] is an unstable dynamic behavior with randomness and ergodicity in deterministic nonlinear systems, which is highly sensitive to system parameters. Based on the strange nonchaotic behavior, it can perform the overall search faster than the probability-dependent random ergodic search. In this study, an strange nonchaotic particle swarm optimization (SNPSO) algorithm is proposed to identify the papermaking process. First, random particles are initialized by strange nonchaotic sequences to obtain high-quality solutions. Furthermore, the weights updating with strange nonchaotic features and time-varying acceleration coefficient are used to improve the global search ability and search speed. Finally, a mutation individual with strange nonchaotic characteristics is utilized to further improve the global search ability. Simulation results demonstrate the effectiveness of the algorithm. To highlight the advantages of the proposed algorithm, a comparative study is also implemented, and it is proved that the convergence speed, global search ability, and robustness of SNPSO are superior to classical PSO [19], PSO with time-varying acceleration coefficients (PSO-TVAC) [29], and modified particle swarm optimization (MPSO) [22].

2 Basis weight control in papermaking process

The evaluation of paper quality includes the basis weight of paper, moisture, ash, color, etc. The basis weight means the weight of paper per unit area expressed in g/m^2. The smaller the basis weight fluctuation, the more uniform the paper, and the better the quality. The control of basis weight includes cross-direction (CD) basis weight control and machine-direction (MD) basis weight control. The CD basis weight control is completed by the headbox dilution water valve, while the MD basis weight control is completed by the pulp pump controlling the pulp flow. The main reasons for the MD basis weight fluctuation are the changes in paper machine speed, pulp amount, pulp concentration, etc. When the paper machine is in normal production, the paper machine speed is stable; therefore, the change in paper machine speed is generally not considered when considering the MD basis weight control. In addition to the above factors, CD basis weight fluctuation also needs to consider the interaction between dilution water valves.

The basis weight control system is illustrated in Fig. 1. The pulp in the pulp tank is transported to the headbox using the pulp pump. The quality control system (QCS) calculates the difference between the value of basis weight measured by the scanner and set value, and the output controls the feeding of the pulp pump to stabilize the pulp amount, so as to achieve the effect of basis weight stability control.

The basis weight control system is a nonlinear, large, time-delay system. Flow, pressure, and other non-linear analog signals are easily subjected to electromagnetic interference during transmission, which is easy to cause detection errors, and then affects the accuracy of the identification model. Time-varying factors such as temperature change, flow jitter, and valve wear make the process object and model time-varying and uncertain. The time delay will greatly increase the control difficulty. With the demand of consumers for high-quality paper and use of advanced control technology, determining a parameter identification method to accurately identify the process model with a small time delay is the key to improving the quality of papermaking process.

3 Principle of parameter identification based on optimization algorithm

The block diagram of system identification based on PSO/Improved PSO (IPSO) is illustrated in Fig. 2.

The purpose is to make the output $y(t)$ of the selected time-delay system approach the output $\hat{y}(t)$ of the real unknown system under the same input signal ($u/(t)$). Thus, the accurate mathematical model of the real unknown system is determined, which lays a foundation for selecting the appropriate control method and designing the control system. In this study, the SNPSO is adopted to identify the unknown parameters of the transfer function FOPDT and SOPDT. The integral of absolute error (IAE) as the performance index is given by:

$$J = \int_0^t \left| e(t) \right| \mathrm{d}t \tag{1}$$

where $e(t) = y(t) - \hat{y}(t)$.

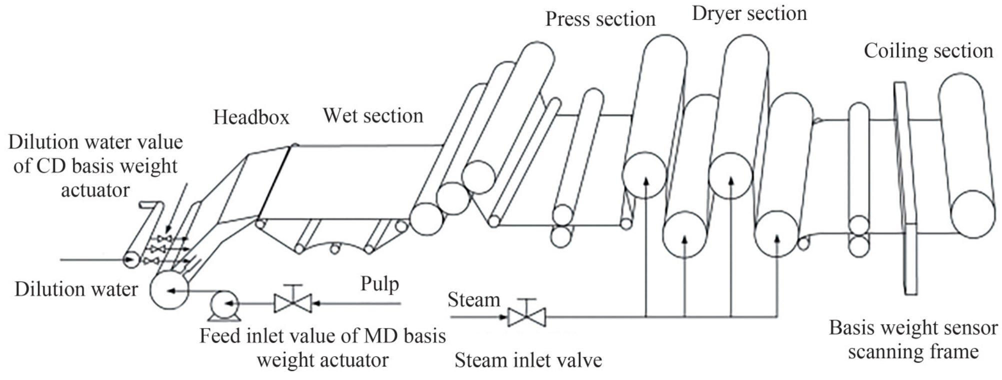

Fig. 1 Structure of basis weight control system

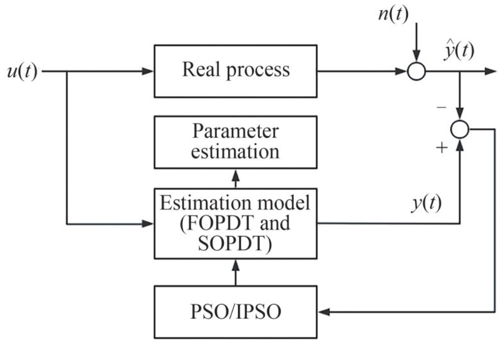

Note: $n(t)$ is noise signal.

Fig. 2 Block diagram of system identification based on PSO/IPSO

4 Review of three PSO strategies

Since the introduction of the PSO method, it has been applied in several applications, such as system identification [19], odor source localization [30], defense against synchronization (SYN) flooding attacks [31–32], and other complex issues [33]. Here, several PSO algorithms are reviewed and become the performance measurement of SNPSO.

4.1 PSO algorithm

PSO is an intelligent search algorithm that mimics the social behavior of birds. Every particle in PSO is initialized at a random position within a given search space. These particles collect and exchange information with each other centered on their location. Furthermore, the positions of these particles are updated at a certain speed according to the effective information. Assuming that the dimension of the search space is N, for particle j, the position vector X_j and velocity vector V_j can be written as $X_j = (x_{j1}, \ldots, x_{jn})$ and $V_j = (v_{j1}, \ldots, v_{jn})$, respectively. The best position $pbest_j$ of the j-th particle is the best previous position that gives the best fitness value, and is expressed as $pbest_j=(p_{j1}, \ldots, p_{jn})$. The best one among all the positions of particles is the global optimal position $gbest$, it is expressed as $gbest=pbest_g=(p_{g1}, \ldots, p_{gN})$. Each particle modifies its position according to a certain speed v_{jn} (n=1, ..., N), and the distance forms the individual optimal and global solutions, $pbest_{jn}$ and $gbest_n$, respectively. The new velocity and position updating equations of each particle in the next iteration are given by:

$$v_{jn}^{k+1} = w^k v_{jn}^k + c_1 r_1 (p_{jn} - x_{jn}) + c_2 r_2 (p_{gn} - x_{jn}) x_{jn}^{k+1} = x_{jn} + v_{jn}^{k+1} \tag{2}$$

where r_1 and r_2 represent random numbers between 0 and 1, c_1 and c_2 are cognitive and social coefficients, w represents the inertia weight that decays linearly with the number of iterations and is expressed as $w=w_{max}-(w_{max}-w_{min})iter/iter_{max}$, $iter$ and $iter_{max}$ represent the current iteration number and maximum number of iterations, respectively, and w_{max} and w_{min} are 0.9 and 0.4, respectively. Fig. 3 illustrates a working principle of PSO, which helps to better understand its operation mode.

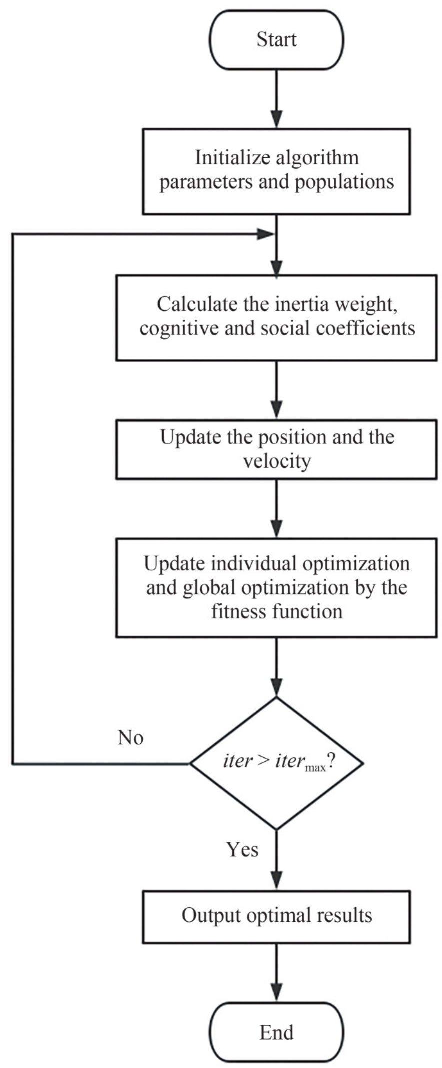

Fig. 3 Flowchart of PSO working principle

4.2 PSO-TVAC algorithm

The time-varying inertia weight can make PSO algorithm converge to the solution with higher accuracy. However, the cognitive coefficient c_1 and social coefficient c_2 are fixed, which is an unfavorable limitation to determine the optimal solution. In Refs. [32−33], the authors introduce two dynamical coefficients to optimize the target. The cognitive coefficient c_1 decreases with the increase in the number of iterations, and the social coefficient c_2 increases with the increase in the number of iterations. This ensures that individuals can fully roam the entire target space in the early stage of search, rather than spend a lot of energy clustering near the local optimal solution. In the later search stage, small cognitive coefficient and large social coefficient encourage the particles to converge to the global optimal state before the end of the search. The dynamical cognitive coefficient c_1 and social coefficient c_2 are expressed as [26]:

$$c_1 = (c_{1f} - c_{1i})iter/iter_{\max} + c_{1i} \tag{3}$$

$$c_2 = (c_{2f} - c_{2i})iter/iter_{\max} + c_{2i} \tag{4}$$

where the cognitive coefficient c_1 decreases from c_{1i} to c_{1f}, and the social coefficient c_2 increases from c_{2i} to c_{2f}. c_{1i} and c_{2f} are set to 2.5, each, while c_{1f} and c_{2i} are set to 0.5, each. In addition, the position updating Eq. (2) is slightly modified as:

$$x_{jn}^{k+1} = x_{jn} + C\,v_{jn}^{k+1} \tag{5}$$

where $C = 2/(2 - \phi - \sqrt{\phi^2 - 4\phi})$; ϕ is set to 4.1.

4.3 MPSO algorithm

The MPSO is introduced in Ref. [19]. The dynamical cognitive coefficient c_1 and social coefficient c_2 are expressed as:

$$c_1 = (c_{1f} - c_{1i})e^{-70\left(\frac{w^k - w_{\min}}{w_{\max} - w_{\min}}\right)^6} + c_{1i} \tag{6}$$

$$c_2 = (c_{2f} - c_{2i})e^{-70\left(\frac{w^k - w_{\min}}{w_{\max} - w_{\min}}\right)^6} + c_{2i} \tag{7}$$

where c_{1i}, c_{1f}, c_{2i}, and c_{2f} are in the range of [0, 4] and c_{1i}> c_{2f}>c_{2i}>c_{1f}. c_{1i} and c_{2f} are set to 1.7, each, while c_{1f} and c_{2i} are set to 1.3, each. In addition, a mutation rule is applied for each particle. If r_3>0.9, then $n=[N \cdot r_4]$ and $x_{jn}= x_{\min}+(x_{\max}-x_{\min})r_5$. r_3, r_4, and r_5 are random values in the range of [0, 1].

5 SNPSO algorithm

A common feature of the above improved PSO algorithm is to improve the convergence accuracy and speed by altering the cognitive and social coefficients, c_1 and c_2, respectively. However, the influence of linear attenuation weight on the algorithm is not considered. For the linear attenuation weight, the change of w completely depends on the current and maximum number of iterations, which leads to slow convergence in the later stage of the iteration. Therefore, it is difficult to jump out of the local optimal solution. In this section, strange nonchaos is introduced into the PSO algorithm and the SNPSO algorithm is developed. Strange nonchaotic behavior is an unpredictable dynamical behavior in nonlinear systems. Mapping this behavior to some parameters in the algorithm will improve the performance of the algorithm.

To obtain strange nonchaotic sequences, a strange nonchaotic system is described as follows [23]:

$$y(n+1) = \begin{cases} v_1 y(n) + a + \varepsilon\cos(2\pi\varphi(n)), \\ if \quad y(n) \leqslant 0 \\ v_2 y(n) + a + \varepsilon\cos(2\pi\varphi(n)) + 1, \\ if \quad y(n) > 0 \end{cases} \tag{8}$$

$$\varphi(n+1) = \varphi(n) + w \bmod (1) \tag{9}$$

There are four unknown parameter values in Eq. (8), which is not conducive for determining strange nonchaotic sequences. Therefore, we first determine the values of parameters v_1 and v_2 via several experiments, reduce the number of unknown variables, and then determine strange nonchaotic sequences using the remaining variable parameters a and ε. v_1 and v_2 are constant parameters and fixed at v_1=0.7 and v_2=1.2, a and ε are bifurcation parameters, n is the number of iterations, w is the frequency and is fixed at $w=(\sqrt{5}-1)/2$. Strange nonchaotic behavior is characterized by the phase diagram and largest Lyapunov exponent. The largest Lyapunov exponent $\lambda_{\max}$ is calculated by:

$$\lambda_x = \lim_{N\to\infty}\frac{1}{N}\sum_{i=1}^{n}\ln\left|\frac{\partial f}{\partial x_i}\right| \tag{10}$$

The bifurcation parameters a and ε are fixed at a= 0.5965 and ε=0.1. Fig. 4(a) illustrates the phase diagram of a fractal attractor, and the largest Lyapunov exponent equals −0.0014 (nonchaotic). Therefore, the fractal attractor is a strange nonchaotic attractor. The strange nonchaotic sequence has features of randomness and non-repetition as illustrated in Fig. 4(b). To obtain

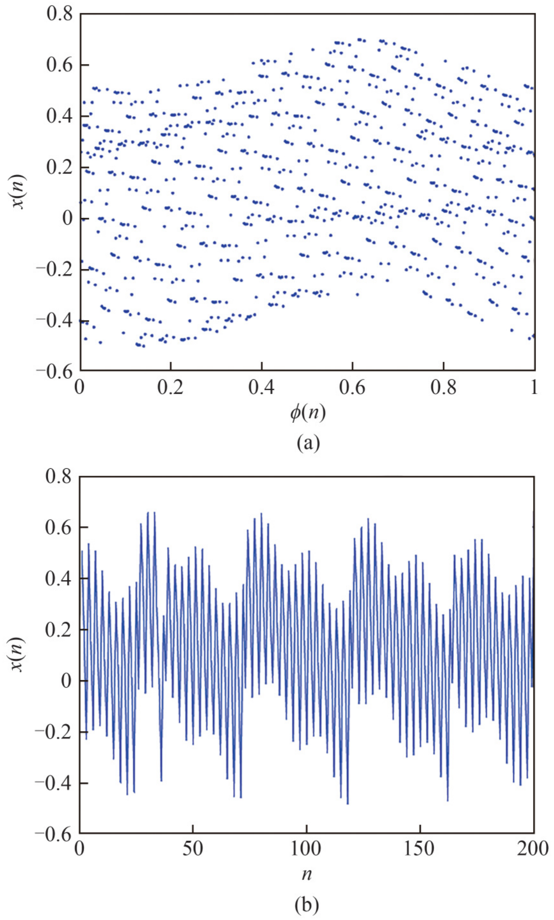

Fig. 4 (a) phase diagram and (b) time sequence diagram of a strange nonchaotic attractor for a=0.5965 and ε=0.1

higher quality initialization particles, the strange nonchaotic sequence is employed to generate particles instead of random generation. Because the random distribution is not affected by external forces, the distribution of strange nonchaotic sequences can be altered according to the change of parameters. Therefore, we can determine a group of strange nonchaotic particles uniformly distributed in the target space, which can overcome the uncertainty of the particle mass of the random sequence. It is also adopted to replace the linear attenuation weight to improve the convergence speed of the algorithm. From Fig. 4(b), we observe that the randomness of strange nonchaotic sequences is different from that of linear decay sequences. The strange nonchaotic sequences will quickly determine a valid value of w_v, and the non-repetition strange nonchaotic sequences will continue to search for a better value of w near the valid value (w_v). Eq. (6) and Eq. (7) are selected as their dynamic coefficients. A mutation rule with strange nonchaotic characteristics is applied for each particle. If r_3>0.9, then n=[N·r_4], $x_{jn}=x_{min}+(x_{max}-x_{min})\hat{y}_j$, and r_3 and r_4 are random values in the range of [0, 1]. $\hat{y}_j$ is the normalized strange nonchaotic sequence. The process of the proposed SNPSO algorithm is illustrated in Fig. 5.

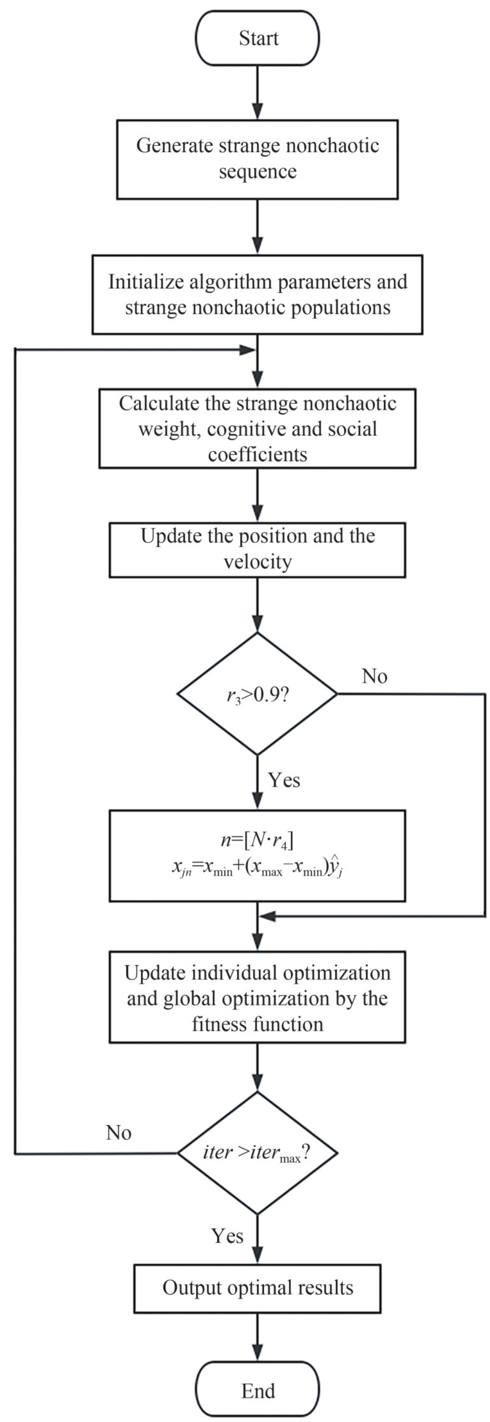

Fig. 5 Flow chart of SNPSO algorithm

6 Simulation experiments

This section aims to study the proposed SNPSO algorithm to address the identification problem of the actual process. Therefore, we choose the FOPDT and SOPDT as the estimation models to approximate the following real process models:

$$P_1(s) = \frac{1}{s+1}e^{-s} \tag{11}$$

$$P_2(s) = \frac{1}{(s+1)^2}e^{-s} \tag{12}$$

$$P_3(s) = \frac{1}{(s+1)^8} \tag{13}$$

$$P_4(s) = \frac{9}{(s+1)(s^2+2s+9)} \tag{14}$$

The inclusion of systems P_1 and P_2 is to confirm that when modeling FOPDT or SOPDT systems with FOPDT or SOPDT models, all the procedures realise an exact match. The identification performance of four algorithms (classical PSO, PSO-TVAC, MPSO, and the proposed SNPSO) is compared. The parameters of four algorithms are set as follows: the sampling time t=20 s; sampling interval σ_t=0.01 s; input is step signal; additive noise is Gaussian white noise with a mean value of 0 and variance of 0.16. The parameters of the four algorithms are presented in Table 1. Matlab R2018a is adopted to perform the above design steps under the environment of Intel(R) Core(TM) i5-4210M CPU@2.60 GHz. In total, 10 independent operations are conducted for each system, and detailed result analysis is described as follows.

Table 1 Parameters of classical PSO, PSO-TVAC, MPSO, and SNPSO

Methods	Population	Maxgen	Inertia weight	Other parameters
Classical PSO	30	100	w_{max}=0.9 w_{min}=0.4	c_1=2 c_2=2
PSO-TVAC	30	100	w_{max}=0.9 w_{min}=0.4	c_{1i}=2.5, c_{1f}=0.5, c_{2i}=0.5, c_{2f}=2.5
MPSO	30	100	w_{max}=0.9 w_{min}=0.4	c_{1i}=1.7, c_{1f}=1.3, c_{2i}=1.3, c_{2f}=1.7
SNPSO	30	100	w_{max}=0.9 w_{min}=0.4	c_{1i}=1.7, c_{1f}=1.3, c_{2i}=1.3, c_{2f}=1.7

6.1 Transfer function P_1

The real process is assumed to be the transfer function (Eq. (11)). The estimation model (FOPDT model) is as follows:

$$G_F(s) = \frac{K_F}{T_F s+1}e^{-L_F s} \tag{15}$$

where the parameters K_F, T_F, and L_F are the estimation parameters. The classical PSO, PSO-TAVC, MPSO, and the proposed SNPSO are adopted to identify the selected estimation model. To verify the identification ability of the above algorithms, experiments are conducted at step response with zero noise, step response with Gaussian noise, and denoised step response. When the output $\hat{y}(t)$ is a step response with zero noise ($n(t)$=0), Table 2 presents the identification accuracy, minimum (min), maximum (max), mean, and standard (std) deviation of the optimal loss function using the four methods ten times, respectively. The accuracy of model identification using the SNPSO algorithm is as high as 90%, which is much higher than the other three algorithms. Fig. 6 illustrates the parameters K_F, T_F, and L_F of the estimation model obtained by running the four algorithms ten times, respectively. The classical PSO, PSO-TAVC, MPSO, and proposed SNPSO algorithms are represented by blue, red, green, and yellow star-lines. SNPSO has excellent average convergence and stability. Fig. 7 illustrates the variations for objective function J using four algorithms. The SNPSO method converges faster and more precisely than other PSO-based algorithms.

Table 2 System identification of FOPTD using four PSO-based algorithms

Methods	Best parameter	Accuracy/%	Min	Max	Mean	Std
Classical PSO	K_F=1, T_F=1, L_F=1	20	0	927	201	300
PSO-TVAC	K_F=1, T_F=1, L_F=1	20	0	3296	432	1023
MPSO	K_F=1, T_F=1, L_F=1	30	0	1072	284	426
SNPSO	K_F=1, T_F=1, L_F=1	90	0	506	50	160

To verify the robustness of the proposed algorithm, a Gaussian white noise $n(t)$ with variance of 0.16 is added to the output $\hat{y}(t)$. Fig. 8 illustrates the parameters K_F, T_F, and L_F of the estimation model obtained from ten experiments using four algorithms. The SNPSO ensures that the proportion of the distance $|K_F-1|<0.004$ is 60%, distance $|T_F-1|<0.4$ is 60%, and distance $|L_F-1|<0.02$ is 80%. The values of three parameters of the estimation model obtained by the other three algorithms

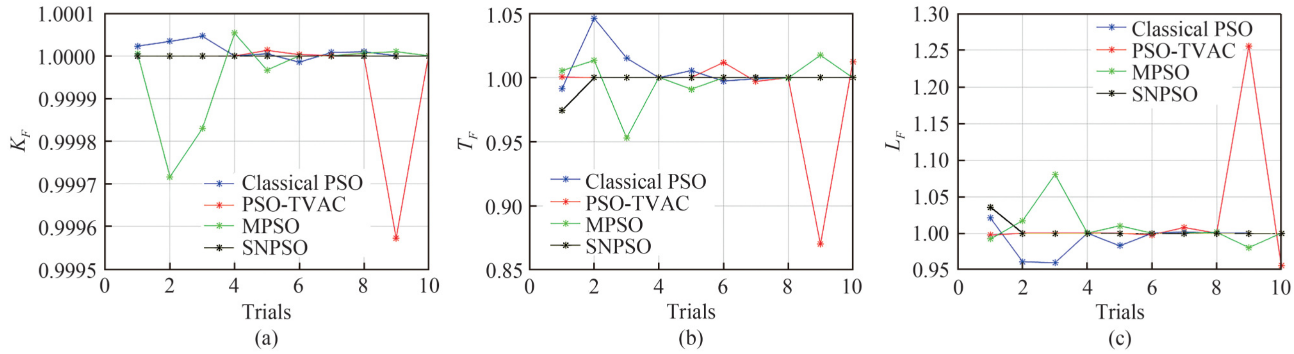

Fig. 6 Identification parameters of FOPTD with zero noise obtained by running the four algorithms ten times

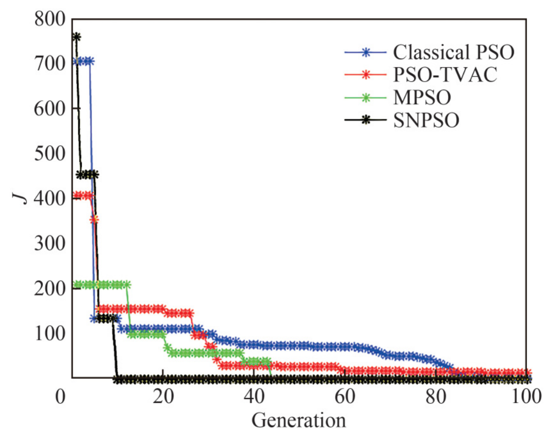

Fig. 7 Variations of objective function J for FOPTD using four algorithms

exceed this range. Therefore, the SNPSO algorithm has excellent robustness in comparison with the other three algorithms. To improve the robustness of the algorithm, the wavelet denoised method is employed to process the signal with noise. The basic idea of wavelet denoising is to remove the wavelet coefficients corresponding to the noise in each frequency band, retain the wavelet decomposition coefficients of the original signal, and then reconstruct the processed coefficients to obtain the pure signal. Fig. 9 illustrates the parameters of the estimation model for identifying the denoised and noised step responses using SNPSO. When denoised

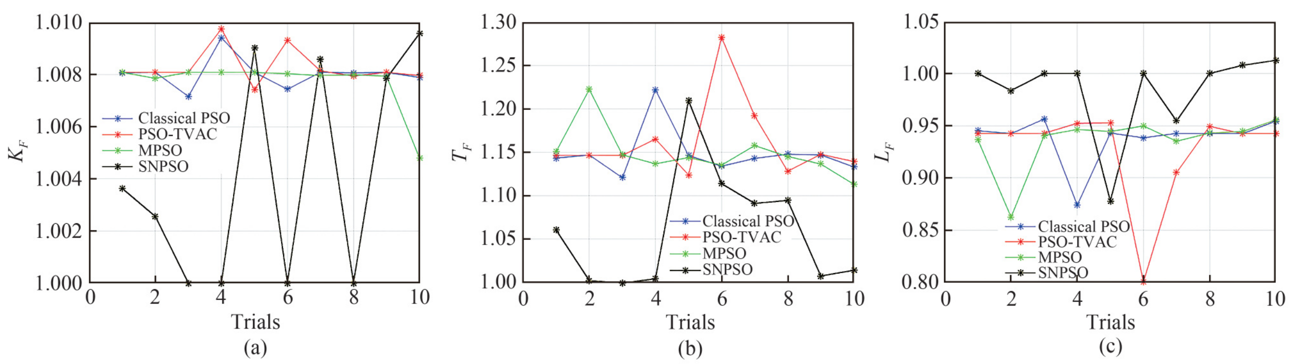

Fig. 8 Identification parameters of FOPTD with Gaussian noise by running the four algorithms ten times

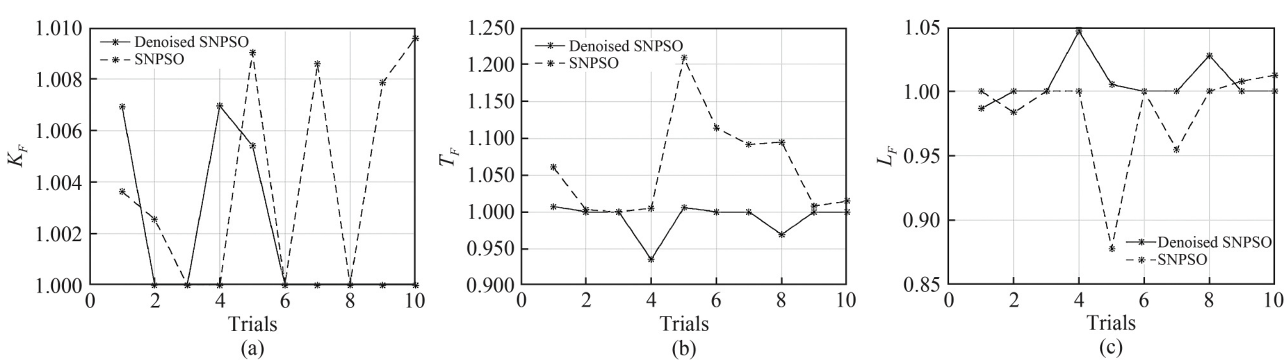

Fig. 9 Identification parameters of denoised FOPTD with Gaussian noise by running the four algorithms ten times

algorithm is adopted for noisy step response, the identification accuracy rates of parameters K_F, T_F, and L_F by SNPSO are increased from 40%, 20%, and 40% to 70%, 60%, and 50%, respectively. It can enhance the stability and robustness of SNPSO.

6.2 Transfer function P_2

When the real process is assumed to be the transfer function (Eq. (12)), the estimation model (SOPTD model) is as follows:

$$G_S(s) = \frac{K_S}{(T_{S1}s+1)(T_{S2}s+1)} e^{-L_S s} \tag{16}$$

Parameters K_S, T_{S1}, T_{S2}, and L_S are the estimation parameters and are characterized by the classical PSO, PSO-TVAC, MPSO, and proposed SNPSO. For zero noise step response $\hat{y}(t)$, Table 3 presents five performance indexes of the four methods. The accuracy and mean of identification (mean) using SNPSO are far better than the other three algorithms. The average convergence and stability of SNPSO are further verified by comparing the parameters K_S, T_{S1}, T_{S2}, and L_S of the estimation model obtained by running the four algorithms ten times (as illustrated in Fig. 10). Fig. 11 illustrates

Table 3 System identification of SOPTD using four PSO-based algorithms

Methods	Best parameter	Accuracy/%	Min	Max	Mean	Std
Classical PSO	K_S=1, T_{S1}=1, T_{S2}=1, L_S=1	10	0	6392	1786	2312
PSO-TVAC	K_S=1, T_{S1}=1, T_{S2}=1, L_S=1	10	0	6714	2112	2470
MPSO	K_S=1, T_{S1}=1, T_{S2}=1, L_S=1	50	0	6352	1242	2048
SNPSO	K_S=1, T_{S1}=1, T_{S2}=1, L_S=1	90	0	6309	630	1995

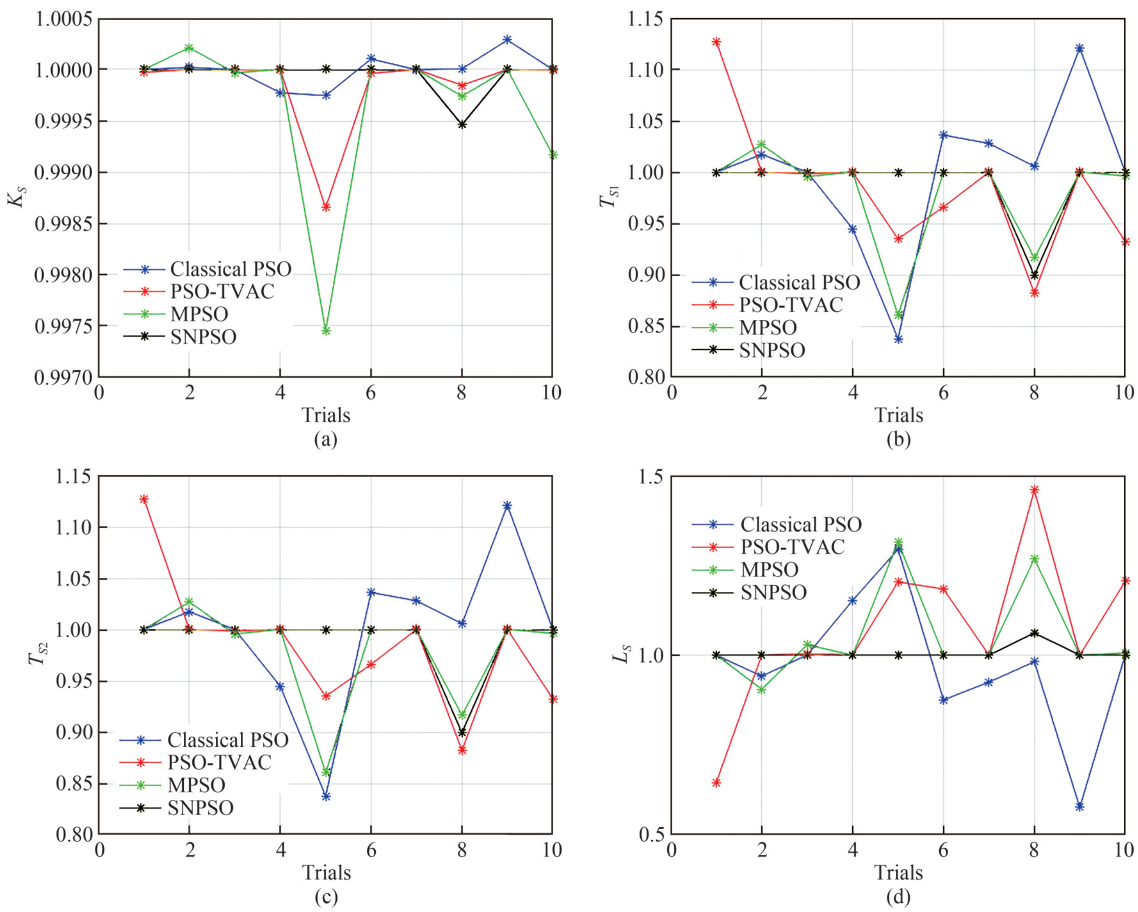

Fig. 10 Identification parameters of SOPTD with zero noise obtained by running the four algorithms ten times

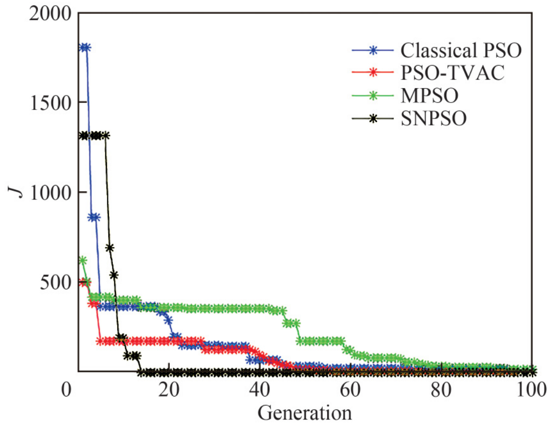

Fig. 11 Variations of objective function J for SOPTD using four algorithms

the variations of objective function J for four algorithms during the optimization. The convergence speed and convergence precision of four PSO-based algorithms is clearly illustrated in this figure. SNPSO method converges faster and more precisely than other PSO-based algorithms.

The noise signal $n(t)$ with variance of 0.16 is added to the output $\hat{y}(t)$ to verify the robustness of the algorithm. Fig. 12 illustrates the SOPTD system parameters K_S, T_{S1}, T_{S2}, and L_S obtained from ten experiments using four algorithms. The parameter value of the estimated system obtained by SNPSO algorithm is closer to the parameter value of the real process. Fig. 13 illustrates that the wavelet denoising method improves the stability and robustness of SNPSO.

6.3 Transfer function P_3

When the real process is assumed to be the transfer function (Eq. (13)) the estimation models are as follows:

$$G_F(s) = \frac{K_F}{T_F s + 1} e^{-L_F s} \tag{17}$$

and

$$G_S(s) = \frac{K_S}{(T_{S1}s + 1)(T_{S2}s + 1)} e^{-L_S s} \tag{18}$$

Table 4 and Table 5 present the FOPDT and SOPDT model parameters for processes P_3, respectively. To compare the identification capabilities of the four

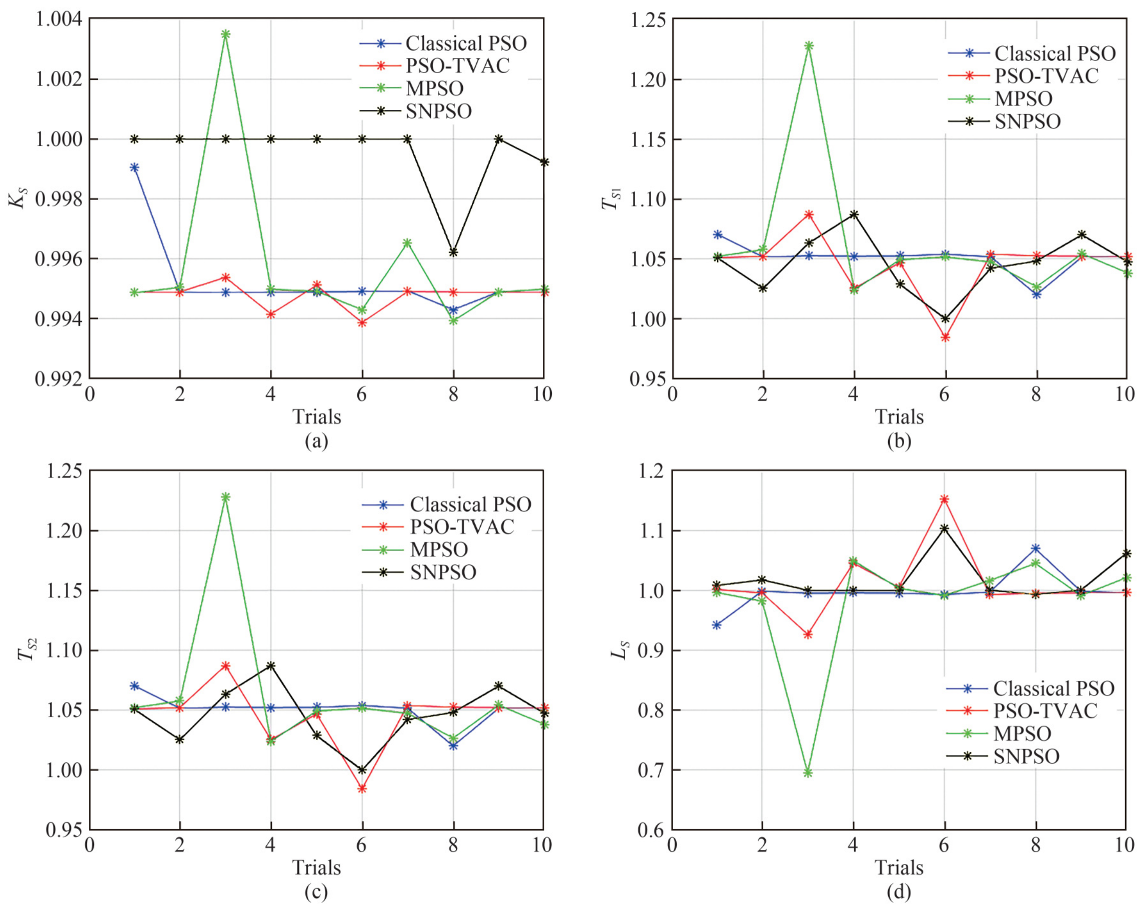

Fig. 12 Identification parameters of SOPTD with Gaussian noise by running the four algorithms ten times

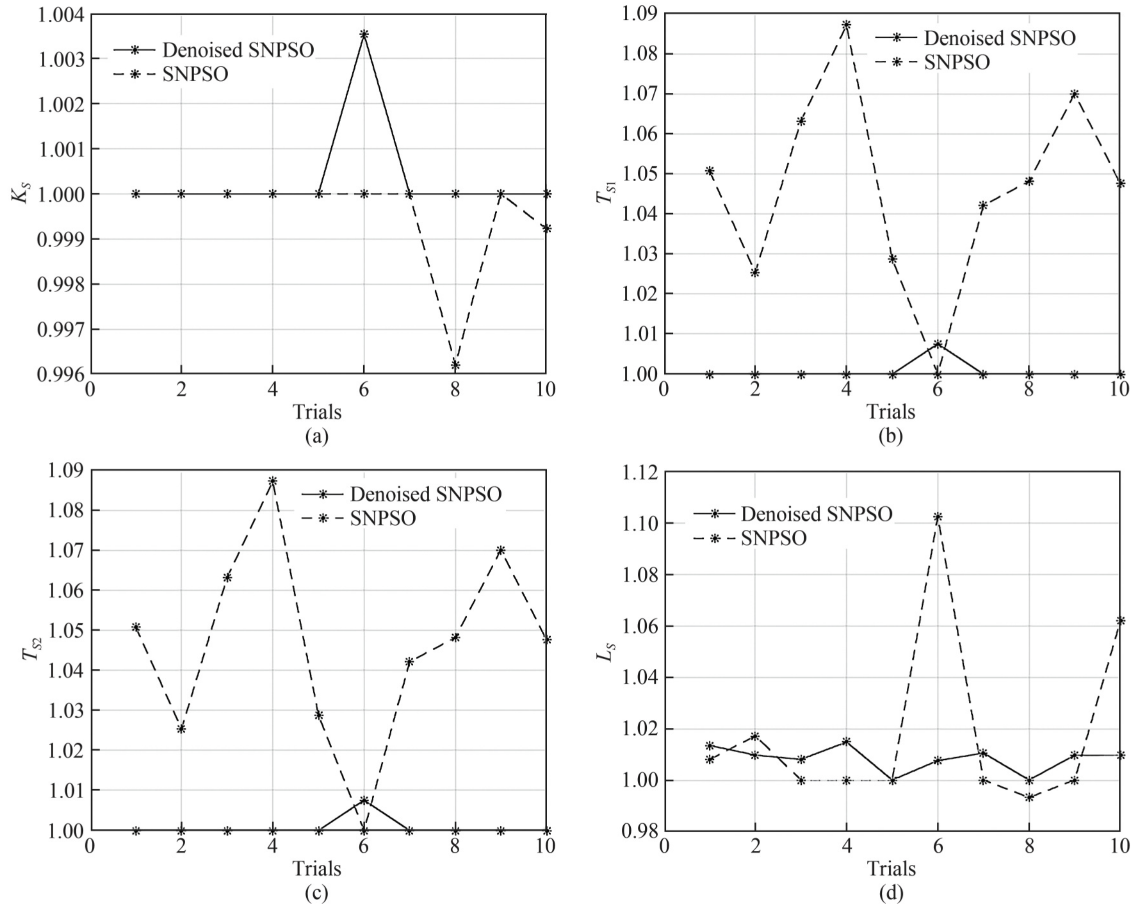

Fig. 13 Identification parameters of denoised SOPTD with Gaussian noise by running the four algorithms ten times

Table 4 FOPDT results for P_3 using four PSO-based algorithms

Methods	Best parameter	Min	Max	Mean	Std
Classical PSO	K_F=1.016, T_F=2.989, L_F=5.473	315.1	1251.7	610.6	371.5
PSO-TVAC	K_F=1.016, T_F=2.991, L_F=5.473	315.1	1251.7	496.9	319.7
MPSO	K_F=1.016, T_F=2.987, L_F=5.476	315.1	500.3	338.1	57.8
SNPSO	K_F=1.016, T_F=2.990, L_F=5.473	315.1	470.3	316.3	51.7

algorithms, the tables also include a measure of performance: the integral of absolute error (IAE), where the error in each case is the difference between the "real" process and model output. The statistical results demonstrate that SNPSO can determine the best

Table 5 SOPDT results for P_3 using four PSO-based algorithms

Methods	Best parameter	Min	Max	Mean	Std
Classical PSO	K_S=1.008, T_{S1}=1.954, T_{S2}=2.069, L_S=4.221	173.5	1323.7	366.3	350.8
PSO-TVAC	K_S=1.008, T_{S1}=2.059, T_{S2}=1.962, L_S=4.234	173.3	2093.7	630.7	627.8
MPSO	K_S=1.009, T_{S1}=1.919, T_{S2}=2.185, L_S=4.149	175.8	1257.1	323.4	317.5
SNPSO	K_S=1.008, T_{S1}=2.011, T_{S2}=2.014, L_S=4.226	173.1	958.4	290.5	290.4

approximation parameters, and the average convergence performance of SNPSO is better than other methods. Fig. 14 and Fig. 15 illustrate the best FOPDT and

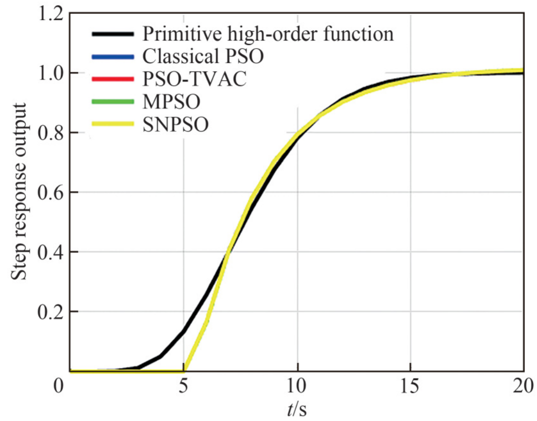

Fig. 14 Step response of the best FOPDT approaching P_3 using classical PSO, PSO-TVAC, MPSO, and SNPSO

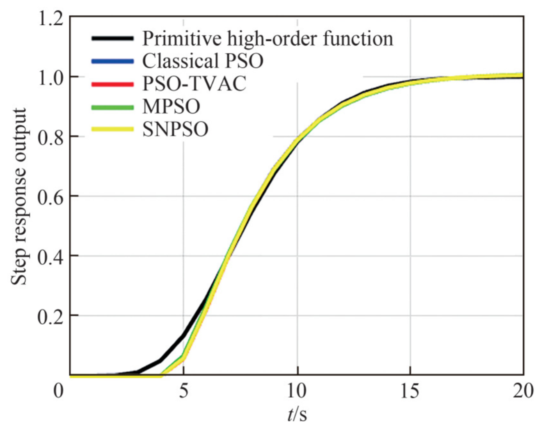

Fig. 15 Step response of the best SOPDT approaching P_3 using classical PSO, PSO-TVAC, MPSO, and SNPSO

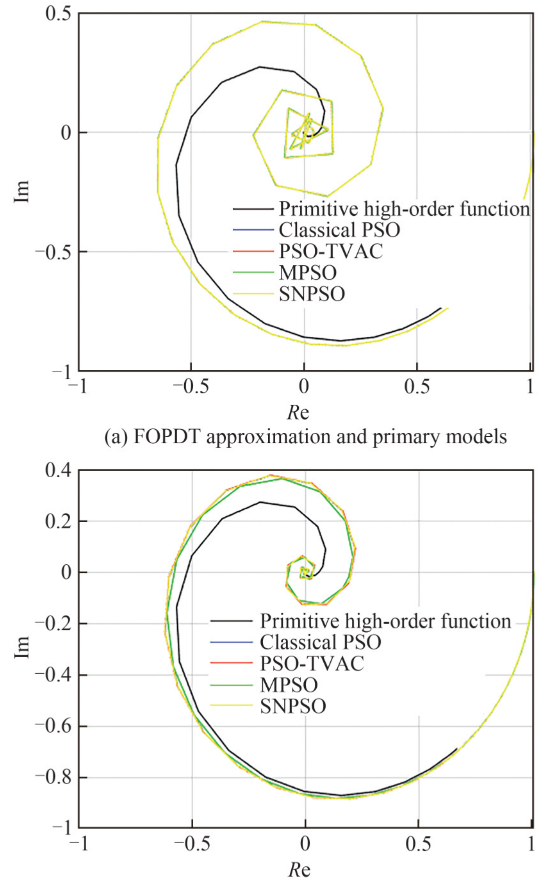

(a) FOPDT approximation and primary models

(b) SOPDT approximation and primary models

Fig. 16 Nyquist curve: primitive high-order function P_3 (black line), and approximation model using PSO (blue), PSO-TVAC, MPSO, and SNPSO

SOPDT step responses approximating P_3 using classical PSO, PSO-TVAC, MPSO, and SNPSO. Black line represents the primitive high-order function P_3. The identification method based on optimization algorithm can make the identification model approach the primary model well. The approximation performance of the SOPDT model is better than that of the FOPDT model. Nyquist curve further proves that the SOPDT model is more approximate to the primary model than the FOPDT model as illustrated in Fig. 16.

6.4 Transfer function P_4

When the real process is assumed to be the transfer function (Eq. (14)), the estimation models are as follows:

$$G_F(s) = \frac{K_F}{T_F s + 1} e^{-L_F s} \tag{19}$$

$$G_S(s) = \frac{K_S}{(T_{S1} s + 1)(T_{S2} s + 1)} e^{-L_S s} \tag{20}$$

Table 6 and Table 7 present the FOPDT and SOPDT model parameters for processes P_4, respectively. To compare the identification capabilities of the four algorithms, the tables also include a measure of

Table 6 FOPDT results for P_4 using four PSO-based algorithms

Methods	Best parameter	Min	Max	Mean	Std
Classical PSO	K_F=1.000, T_F=0.919, L_F=0.294	22.3	2331.2	290.9	718.5
PSO-TVAC	K_F=1.000, T_F=0.921, L_F=0.318	22.2	4887.8	1119.0	1774.5
MPSO	K_F=1.000, T_F=0.873, L_F=0.360	23.0	236.7	53.0	66.1
SNPSO	K_F=1.000, T_F=0.974, L_F=0.243	22.9	104.1	43.7	29.5

Table 7 SOPDT results for P_4 using four PSO-based algorithms

Methods	Best parameter	Min	Max	Mean	Std
Classical PSO	K_S=1.000, T_{S1}=0.996, T_{S2}=0.221, L_S=0.000	23.6	2908.1	354.2	902.6
PSO-TVAC	K_S=1.000, T_{S1}=0.000, T_{S2}=1.036, L_S=0.000	26.5	2908.1	622.0	1091.5
MPSO	K_S=1.000, T_{S1}=0.935, T_{S2}=0.022, L_S=0.294	22.3	2128.4	558.4	751.6
SNPSO	K_S=1.000, T_{S1}=0.000, T_{S2}=0.910, L_S=0.354	22.3	1648.2	324.8	512.1

performance: the integral of absolute error (IAE), where the error in each case is the difference between the "real" process and model output. The statistical results demonstrate that the average convergence performance of SNPSO is better than other methods. Fig. 17 and Fig. 18 illustrate the best FOPDT and SOPDT step responses approximating P_4 using classical PSO, PSO-TVAC, MPSO, and SNPSO. Black line represents the primitive high-order function P_4. The identification method based on optimization algorithm can make the identification model approach the primary model well. The approximation performance of the FOPDT model is better than that of the SOPDT model. Nyquist curve further proves that the FOPDT model is more

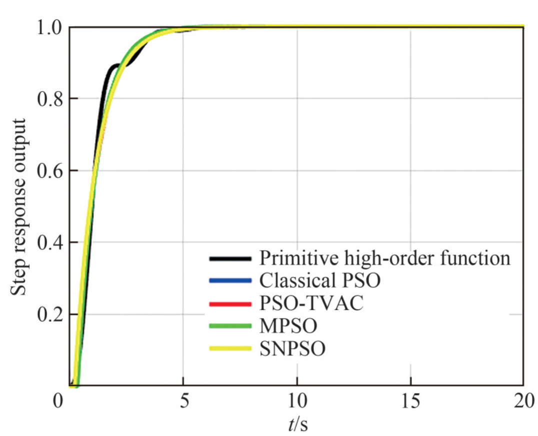

Fig. 17 Step response of the best FOPDT approaching P_4 using classical PSO, PSO-TVAC, MPSO, and SNPSO

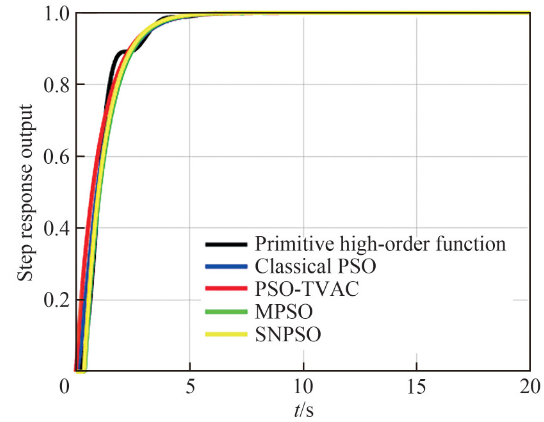

Fig. 18 Step response of the best SOPDT approaching P_4 using classical PSO, PSO-TVAC, MPSO, and SNPSO

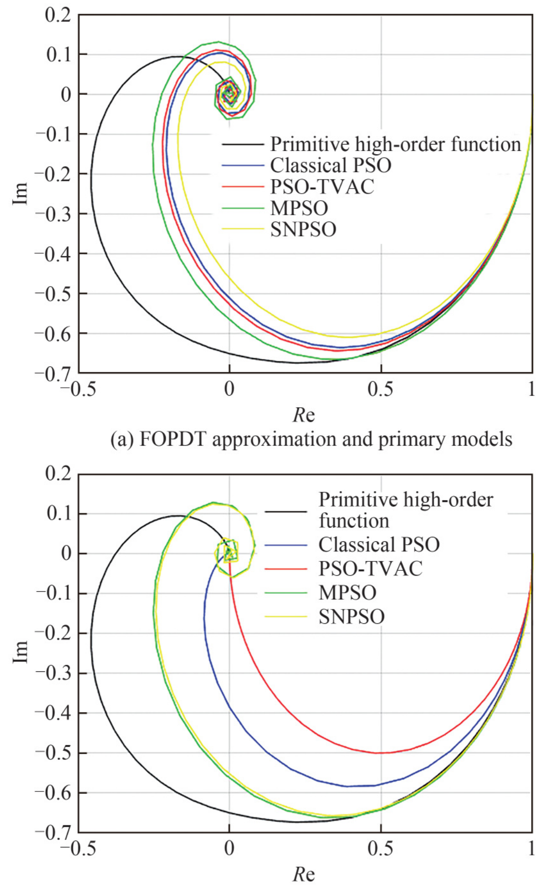

(b) SOPDT approximation and primary models

Fig. 19 Nyquist curve: primitive high-order function P_4 (black line), and approximation model using PSO, PSO-TVAC, MPSO, and SNPSO

approximate to the primary model than the SOPDT model as illustrated in Fig. 19.

7 Conclusions

Here, we introduced the application of the strange nonchaotic particle swarm optimization (SNPSO) algorithm in developing a novel method for identifying the optimal parameters of systems with time delay. Based on the randomness and ergodicity of strange nonchaotic dynamics, the strange nonchaotic sequence was adopted to replace the initialized random particles and linear attenuation weight to improve the global search capability. Furthermore, a mutation rule with strange nonchaotic characteristics was employed to improve global search capability further. To illustrate the effectiveness of SNPSO, it was compared with the other three algorithms (classical particle swarm optimization (PSO), PSO with time-varying acceleration coefficients (PSO-TVAC), and modified particle swarm optimization (MPSO)). Simulation results demonstrated that SNPSO is more suitable for parameter identification of systems with time delay. When the first-order-plus-dead-time (FOPDT) or second-order-plus-dead-time (SOPDT) models were employed to model the FOPDT or SOPDT systems, SNPSO achieved the highest accuracy of accurate matching. To identify high-order systems, SNPSO had the best average and best minimum convergence performances.

Acknowledgments

The authors are grateful for the financial support received from the National Natural Science Foundation of China (Grant No. 62073206) and Technical Innovation Guidance Project of Shaanxi Province (Grant No. 2020CGHJ-007).

References

[1] Ammar M E, Dumont G. Identification of paper machines cross-directional models in closed-loop. In the 2013 5th International Conference on Modelling, Identification and Control (ICMIC) ICMIC, Cairo, Egypt: 2013, 3-9.

[2] Sun G, Nie H, Su Y, Nie W. Research on two-degree-of-freedom IMC-PID control for time-delay systems. *Application Research of Computers*, 2014, 31(8), 2357-2360.

[3] Shan W, Tang W, Wang M, Liu B. Two-degree-of-freedom smith predictor based on fractional order PID controller in paper basis weight. *Packaging Engineering*, 2017, 38(11), 143-147.

[4] Xu Y, Chen D. Partially-linear least-squares regularized regression for system identification. *IEEE Transactions on Automatic Control*, 2009, 54(11), 2637-2641.

[5] Chen T, Ljung L. Implementation of algorithms for tuning parameters in regularized least squares problems in system identification. *Automatica*, 2013, 49(7), 2213-2220.

[6] Poinot T, Trigeassou J C. Identification of fractional systems using an output-error technique. *Nonlinear Dynamics*, 2004, 38(1/4), 133-154.

[7] Silva W. Identification of nonlinear aeroelastic systems based on the volterra theory: progress and opportunities. *Nonlinear Dynamics*, 2005, 39(1/2), 25-62.

[8] Gibson S, Wills A, Ninness B. Maximum-likelihood parameter estimation of bilinear systems. *IEEE Transactions on Automatic Control*, 2005, 50(10), 1581-1596.

[9] Soderstrom T, Hong M, Schoukens J, Pintelon R. Accuracy analysis of time domain maximum likelihood method and sample maximum likelihood method for errors-in-variables and output error identification. *Automatica*, 2010, 46(4), 721-727.

[10] Gu Y, Ding R. A least squares identification algorithm for a state space model with multi-state delays. *Applied Mathematics Letters*, 2013, 26(7), 748-753.

[11] Tao L, Gao F. A frequency domain step response identification method for continuous-time processes with time delay. *Journal of Process Control*, 2010, 20(7), 800-809.

[12] Na J, Ren X, Xia Y. Adaptive parameter identification of linear SISO systems with unknown time-delay. *Systems & Control Letters*, 2014, 66, 43-50.

[13] Ahandani M A, Abbasfam J, Kharrati H. Parameter identification of permanent magnet synchronous motors using quasi-opposition-based particle swarm optimization and hybrid chaotic particle swarm optimization algorithms. *Applied Intelligence*, 2022, 52, 13082-13096.

[14] Zhu M, Axel H, Wen Y. Identification-based controller design using cloud model for course-keeping of ships in waves. *Engineering Applications of Artificial Intelligence*, 2018, 75, 22-35.

[15] Lagos-Eulogio P, Seck-Tuoh-Mora J C, Hernandez-Romero N, Medina-Marin J. A new design method for adaptive IIR system identification using hybrid CPSO and DE. *Nonlinear Dynamics*, 2017, 88(4), 2371-2389.

[16] Prawin J, Rao A, Lakshmi K. Nonlinear parametric identification strategy combining reverse path and hybrid dynamic quantum particle swarm optimization. *Nonlinear Dynamics*, 2015, 84(4), 797-815.

[17] Peng Y, He S, Sun K. Parameter identification for discrete memristive chaotic map using adaptive differential evolution algorithm. *Nonlinear Dynamics*, 2021, 107(1), 1263-1275.

[18] Wang J, Xu Y, She C, Xu P, Bagal H A. Optimal parameter identification of SOFC model using modified gray wolf optimization algorithm. *Energy*, 2022, DOI: 10.1016/j.energy.2021.122800.

[19] Kennedy J, Eberhart R. Particle swarm optimization. *IEEE*

Conference on Neural Networks, 1995, 4, 1942-1948.

[20] Cox C, Tindle J, Burn K. A comparison of software-based approaches to identifying FOPDT and SOPDT model parameters from process step response data. *Applied Mathematical Modelling*, 2016, 40(1), 100-114.

[21] Zou D, Deb S, Wang G. Solving IIR system identification by a variant of particle swarm optimization. *Neural Computing and Applications*, 2018, 30(3), 685-698.

[22] Feng Y, Li Y, Liang M. System Identification of micro piezoelectric actuators via rate-dependent prandtl-ishlinskii hysteresis model based on a modified PSO algorithm. *IEEE Transactions on Nanotechnology*, 2020, DOI: 10.1109/TNANO.2020.3034965.

[23] Shen Y, Zhang Y. Mechanisms of strange nonchaotic attractors in a nonsmooth system with border-collision bifurcations. *Nonlinear Dynamics*, 2019, 96(2), 1405-1428.

[24] Danca M F, Feckan M, Kuznetsov N, Chen G. Rich dynamics and anticontrol of extinction in a prey-predator system. *Nonlinear Dynamics*, 2019, 98(2), 1421-1445.

[25] Yuan Y, Miao P, Xie J. Coexistence of strange nonchaotic attractors and a special mixed attractor caused by a new intermittency in a periodically driven vibro-impact system. *Nonlinear Dynamics*, 2017, 87(2), 1-21.

[26] Shen Y, Zhang Y. Strange nonchaotic attractors in a quasiperiodically-forced piecewise smooth system with farey tree. *Fractals*, 2019, DOI: 10.1142/S0218348X19501184.

[27] Li G, Yue Y, Grebogi C, Li D, Xie J. Strange nonchaotic attractors and multistability in a two-degree-of-freedom quasiperiodically forced vibro-impact system. *Fractals*, 2021, DOI: 10.1142/S0218348X21501036.

[28] Zhang Y, Shen Y. A new route to strange nonchaotic attractors in an interval map. *International Journal of Bifurcation and Chaos*, 2020, DOI: 10.1142/S0218127420500637.

[29] Mohammadi-Ivatloo B, Moradi-Dalvand M, Rabiee A. Combined heat and power economic dispatch problem solution using particle swarm optimization with time varying acceleration coefficients. *Electric Power Systems Research*, 2013, 95, 9-18.

[30] Lu Q, Han Q, Liu S. A finite-time particle swarm optimization algorithm for odor source localization. *Information Sciences*, 2014, 277(1), 111-140.

[31] Ahmed Z, Mahbub M, Jahan S. Defense against SYN flood attack using LPTR-PSO: a three phased scheduling approach. *International Journal of Advanced Computer Science and Applications*, 2017, 8(9), 433-441.

[32] Jamali S, Shaker V. Defense against SYN flooding attacks: a particle swarm optimization approach. *Computers & Electrical Engineering*, 2014, 40(6), 2013-2025.

[33] Gaxiola F, Melin P, Valdez F, Castro J R, Castillo O. Optimization of type-2 fuzzy weights in backpropagation learning for neural networks using GAs and PSO. *Applied Soft Computing*, 2016, 38, 860-871. PBM